

Structure of Polyelectrolyte Solutions at a Charged Surface

Chandra N. Patra

Theoretical Chemistry Section, RC & CD Division, Chemistry Group, Bhabha Atomic Research Centre, Mumbai 400 085, India

Rakwoo Chang and Arun Yethiraj*

Theoretical Chemistry Institute and Department of Chemistry, University of Wisconsin, Madison, Wisconsin 53706

Received: November 2, 2003; In Final Form: April 1, 2004

The structure of polyelectrolyte solutions at a charged surface is studied using density functional theory and Monte Carlo simulations. The polymer molecules are modeled as freely jointed chains of charged hard spheres, the counterions and co-ions as charged hard spheres, and the surface is a planar, impenetrable hard wall with a uniform surface charge density. The density functional theory treats the ideal gas contribution exactly, uses a weighted density approximation for the hard sphere contribution, and a generalized van der Waals approximation for the electrostatic contribution. At a fixed surface charge density, with increasing concentration of the polyanion, the simulations show layering as well as charge inversion phenomena resulting from an interplay between excluded volume and electrostatic interactions. The integrated surface excess is a monotonically decreasing function of polymer concentration at high surface charge densities, but a nonmonotonic function of polymer concentration at lower surface charge densities. The density functional theory is in qualitative agreement with simulations for the density profiles but fails to capture the layering and charge inversion effects. This suggests that liquid-state correlations and coupling between electrostatic and excluded volume effects are important factors in the adsorption of charged polymers at surfaces.

I. Introduction

The adsorption of polyelectrolytes to surfaces has attracted a great deal of interest in recent years because of numerous applications to technologically important problems^{1–3} and relevance to biological systems.^{4–6} One application is in the synthesis of multilayer polyelectrolyte films on solid surfaces, a bottom-up strategy for the fabrication of soft materials for nanotechnology.⁷ These films are made by sequentially adsorbing, layer-by-layer, positively and negatively charged polyelectrolytes onto a charged surface. The potential applications of these possibly multifunctional nanocomposites are enormous, for example, in corrosion-resistant coatings,⁸ in drug delivery, in microreaction cages,⁹ in ultrathin selective membranes,¹⁰ tailoring of optical properties of films, and as biological sensors.¹¹ The mechanism of polyelectrolyte adsorption or layer-by-layer assembly is far from understood. In fact, the adsorption of polyelectrolytes at oppositely charged surfaces¹² is a challenging problem in itself, and not considered to be well understood. In this paper, we study the behavior of salt-free polyelectrolyte solutions at charged surfaces using theory and computer simulation.

There have been a number of theoretical studies of polyelectrolyte adsorption using a variety of techniques. These include solutions of linearized mean-field equations,^{13,14} numerical solutions of full mean-field equations,¹⁵ scaling theories for single-chain adsorption,^{16,17} and formulation of a phenomenological criterion describing the adsorption-depletion transition from charged surfaces.^{18,19} Other approaches employed are the multi-Stern layer models,^{20,21} where a discrete lattice is used

and each lattice site can be occupied by either a monomer, a solvent molecule, or a small ion. The electrostatic potential can then be calculated self-consistently together with the concentrations of the monomers and counterions. An integral equation theory for polyelectrolyte solutions between surfaces has also been reported,²² although the counterions were not explicitly incorporated in that work. While these theoretical approaches might be adequate for weakly coupled systems, e.g., where only monovalent ions are present, they are expected to be inadequate in strongly coupled systems, e.g., where divalent and multivalent ions are present and correlation effects are significant. Correlation effects cannot be easily incorporated into mean field theories, and almost all systems of biological interest involve divalent ions such as Mg^{2+} or Ca^{2+} .

A study of simple models of polyelectrolytes at surfaces using computer simulation and liquid state theory is of considerable interest. Computer simulations have been used extensively to study the density profiles and conformational properties of polymers at interfaces^{23–25} and bulk polyelectrolyte solutions.^{26–30} The simulations provide data against which the accuracy of theories may be tested. Liquid state theoretical approaches are also appealing because computer simulations become prohibitively expensive for long-chain polymers. Density functional theory (DFT) and integral equations have been applied in different forms for the prediction of structure of uniform and nonuniform polymers^{31–38} and also to study the structural and thermodynamic aspects of counterion distribution around a cylindrical polyanion such as DNA.^{39,40}

In this work, we investigate the behavior of polyelectrolyte solutions between charged surfaces using Monte Carlo (MC) simulations and DFT. The polymer molecules are modeled as a “pearl necklace” of freely jointed charged hard spheres, with

* Corresponding author. E-mail: yethiraj@chem.wisc.edu

a negative charge on each sphere, and the surfaces are smooth and carry a uniform (positive) charge density. The counterions (to the polymers) and co-ions are monovalent charged hard spheres with positive and negative charge, respectively. In the free energy functional the ideal gas term is incorporated exactly, the hard sphere chain contribution is treated using the weighted density approximation, and the electrostatic contribution is treated using a van der Waals approximation. For the surface charge densities investigated, the polymers are found in excess near the surface compared to the bulk, as expected. The polymer density profile from the simulations is not a monotonically decreasing function of the distance from the surface, however, and entropic and correlation effects play a significant role at all polymer concentrations investigated. This behavior is missed by the DFT, which predicts the qualitative trends correctly but does not capture the oscillations in the polymer density profiles seen in the simulations. The DFT is more accurate for the integrated surface excess, although it does not predict the nonmonotonic dependence of surface excess on polymer concentrations that is observed in the simulations at the highest value of surface charge density investigated.

The remainder of this paper is organized as follows: in section II we present the molecular model, in section III we formulate the density functional theory for the present system, in section IV we discuss the simulation procedure, and in section V we present results of numerical calculations and compare them with simulations. Finally, we offer a few concluding remarks in section VI.

II. Molecular Model

The model system consists of polyions, counterions, and co-ions confined between two infinite parallel walls. The interaction potential between any two sites, $v(r)$, is given by the sum of a hard sphere and Coulomb interaction

$$\beta v(r) = \infty \quad \text{for } r < d \quad (1)$$

$$= l_B \frac{q_i q_j}{r} \quad \text{for } r > d \quad (2)$$

where r is the distance between two sites, q_i is the valence of species i ($q_i = -1$ for polymer sites, $+1$ for counterion sites, and -1 for co-ion sites), $\beta = 1/k_B T$, k_B is Boltzmann's constant, T is the temperature, $l_B = \beta e^2 / \epsilon$ is the Bjerrum length, and ϵ is the dielectric constant of the solvent. Adjacent sites along the polymer backbone are constrained to be at a fixed separation, d . The intramolecular potential, $V(\mathbf{R})$, is therefore given by

$$V(\mathbf{R}) = \sum_{i=2}^{N_m} \sum_{j=1}^{i-1} v(r_{ij}) + \sum_{j=2}^{N_m} v_b(|\mathbf{r}_j - \mathbf{r}_{j-1}|) \quad (3)$$

where \mathbf{R} denotes the positions of all the N_m monomers (or sites) on a polymer molecule, i.e., $\mathbf{R} = \{\mathbf{r}_i\}$, where \mathbf{r}_i is the position of the i th bead of the polymer and v_b constrains adjacent beads to a fixed separation d .

The surface is modeled as a perfectly smooth impenetrable planar wall carrying a uniform surface charge density σ . The interaction potential, $\psi_i(z)$, between the wall and an ion is given by

$$\beta \psi_i(z) = \infty \quad \text{for } z < d \quad (4)$$

$$= -2\pi q_i l_B \frac{\sigma}{\epsilon} z \quad \text{for } z > d \quad (5)$$

III. Density Functional Theory

The central goal of a density functional approach is to find a suitable expression for the grand potential Ω , or equivalently,

the Helmholtz free energy, F , as a functional of the density distributions. The grand potential functional and the Helmholtz free energy functional are related via a Legendre transform:

$$\Omega[\rho_M(\mathbf{R}), \{\rho_\alpha(\mathbf{r})\}] = F[\rho_M(\mathbf{R}), \{\rho_\alpha(\mathbf{r})\}] + \int [\Psi_M(\mathbf{R}) - \mu_M] \rho_M(\mathbf{R}) d\mathbf{R} + \sum_\alpha \int [\psi_\alpha(\mathbf{r}) - \mu_\alpha] \rho_\alpha(\mathbf{r}) d\mathbf{r} \quad (6)$$

where $\rho_M(\mathbf{R})$ is the molecular density of the polymer molecule as a function of the set of site positions $\mathbf{R} (\equiv \{\mathbf{r}_i\})$ where \mathbf{r}_i is the position of site i , $\rho_\alpha(\mathbf{r})$ is the density of component α (the symbol α indicates counterion or coion), μ_M is the chemical potential of the polymer, μ_α is the chemical potential of the component α , and $\Psi_M(\mathbf{R})$ and $\psi_\alpha(\mathbf{r})$ are, respectively, the external potentials on a polymer molecule and on component α . The external potential acting on a polymer molecule is equal to the sum of the potentials on the individual sites: $\Psi_M(\mathbf{R}) = \sum_{i=1}^{N_m} \psi_i(\mathbf{r}_i)$. At equilibrium, Ω is minimum with respect to variations in the density distribution, i.e.,

$$\frac{\delta \Omega}{\delta \rho_M(\mathbf{R})} = \frac{\delta \Omega}{\delta \rho_\alpha(\mathbf{r})} = 0 \quad (7)$$

and this condition is used to determine $\rho_M(\mathbf{R})$ as well as $\rho_\alpha(\mathbf{r})$ and subsequently the grand potential and the Helmholtz free energy.

The free energy functional $F[\rho_M, \{\rho_\alpha\}]$ can, in principle, be expressed as the sum of an ideal gas term (F_{id}) and an excess part (F_{ex}), i.e.,

$$F[\rho_M(\mathbf{R}), \{\rho_\alpha(\mathbf{r})\}] = F_{id}[\rho_M(\mathbf{R}), \{\rho_\alpha(\mathbf{r})\}] + F_{ex}[\rho(\mathbf{r}), \{\rho_\alpha(\mathbf{r})\}] \quad (8)$$

The ideal gas functional is known exactly and is given by

$$F_{id}[\rho_M(\mathbf{R}), \{\rho_\alpha(\mathbf{r})\}] = \beta^{-1} \int d\mathbf{R} \rho_M(\mathbf{R}) [\ln \rho_M(\mathbf{R}) - 1] + \int d\mathbf{R} V(\mathbf{R}) \rho_M(\mathbf{R}) + \beta^{-1} \sum_\alpha \int d\mathbf{r} \rho_\alpha(\mathbf{r}) [\ln \rho_\alpha(\mathbf{r}) - 1] \quad (9)$$

where $V(\mathbf{R})$ is given by eq 3, and the excess free energy F_{ex} is assumed (without loss of generality)^{41,42} to be a functional of only the site densities, $\rho_\alpha(\mathbf{r})$ and $\rho(\mathbf{r})$, with the latter defined as

$$\rho(\mathbf{r}) = \sum_{i=1}^{N_m} \rho_{si}(\mathbf{r}) = \int d\mathbf{R} \sum_{i=1}^{N_m} \delta(\mathbf{r} - \mathbf{r}_i) \rho_M(\mathbf{R}) \quad (10)$$

where $\rho_{si}(\mathbf{r})$ refers to the local density of the site i . The main ingredients of the DFT are an approximation for F_{ex} and an algorithm for minimizing Ω .

The excess free energy functional F_{ex} can be divided into two contributions, one arising from the hard core interactions in a mixture of hard chains and hard spheres (denoted F_{hchs}) and the second (electrical) contribution (denoted F_{el}) arising from the direct Coulomb part, i.e.,

$$F_{ex}[\rho(\mathbf{r}), \{\rho_\alpha(\mathbf{r})\}] = F_{hchs}[\rho(\mathbf{r}), \{\rho_\alpha(\mathbf{r})\}] + F_{el}[\rho(\mathbf{r}), \{\rho_\alpha(\mathbf{r})\}] \quad (11)$$

The above equation is formally exact, although expressions for the excess free energy functionals are not known. In this work, we use the weighted density approximation for F_{hchs} and the generalized van der Waals approximation for F_{el} .

In the weighted density approximation (WDA) for hard chain hard sphere mixtures, F_{hchs} is given by

$$F_{\text{hchs}}[\rho(\mathbf{r}), \{\rho_\alpha(\mathbf{r})\}] = \int \rho(\mathbf{r}) f_{\text{hc}}(\bar{\rho}_{\text{hchs}}(\mathbf{r})) d\mathbf{r} + \sum_\alpha \int \rho_\alpha(\mathbf{r}) f_{\text{hs}}(\bar{\rho}_{\text{hchs}}(\mathbf{r})) d\mathbf{r} \quad (12)$$

where $f_{\text{hc}}(\rho)$ is the excess free energy density due to the neutral bulk polymer and $f_{\text{hs}}(\rho)$ is the excess free energy density due to bulk hard sphere fluid, both evaluated at a density ρ . The total weighted density $\bar{\rho}_{\text{hchs}}(\mathbf{r})$ is given by

$$\bar{\rho}_{\text{hchs}}(\mathbf{r}) = \int [\rho(\mathbf{r}') + \sum_\alpha \rho_\alpha(\mathbf{r}')] w(|\mathbf{r} - \mathbf{r}'|) d\mathbf{r}' \quad (13)$$

where $w(r)$ is the weight function, normalized so that $\int w(\mathbf{r}) d\mathbf{r} = 1$. We use a simple choice for the weighting function,^{43,44} i.e.,

$$w(r) = \frac{3}{4\pi d^3} \Theta(d - r) \quad (14)$$

where $\Theta(r)$ is the Heaviside step function. More sophisticated choices of the weight function involving two-particle correlation function are possible,³³ although that does not result in significantly better results for hard-sphere chains. The quantities $f_{\text{hc}}(\rho)$ and $f_{\text{hs}}(\rho)$ are obtained from the generalized Flory dimer equation of state³¹ and Carnahan–Starling equation of state,⁴⁵ respectively. Note that the contributions to the free energy from each of the species are evaluated at the *total* density of the liquid, and not at the density of the species, because the volume required to insert a sphere is expected to be a function of the total number of spheres. This version of polymeric WDA has been shown⁴⁶ to be quantitatively accurate (when compared to computer simulations) for the density profiles of hard-sphere hard-chain mixtures at hard walls.

In the generalized van der Waals (GvdW) approximation, F_{el} is given by

$$F_{\text{el}}[\rho(\mathbf{r}), \{\rho_\alpha(\mathbf{r})\}] = \frac{1}{2} \sum_{ij} \int \int d\mathbf{r} d\mathbf{r}' \rho_{si}(\mathbf{r}) \rho_{sj}(\mathbf{r}') \frac{q_i q_j}{\epsilon |\mathbf{r} - \mathbf{r}'|} + \frac{1}{2} \sum_{i\alpha} \int \int d\mathbf{r} d\mathbf{r}' \rho_{si}(\mathbf{r}) \rho_\alpha(\mathbf{r}') \frac{q_i q_\alpha}{\epsilon |\mathbf{r} - \mathbf{r}'|} + \frac{1}{2} \sum_{\alpha\alpha'} \int \int d\mathbf{r} d\mathbf{r}' \rho_\alpha(\mathbf{r}) \rho_{\alpha'}(\mathbf{r}') \frac{q_\alpha q_{\alpha'}}{\epsilon |\mathbf{r} - \mathbf{r}'|} \quad (15)$$

where the symbols i and j refer to the sites of the polyions and α, α' refer to the small ions (counterions and co-ions).

A minimization of the grand potential according to the condition of eq 7 yields the following equations for the density profiles:

$$\rho(\mathbf{r}) = \int d\mathbf{R} \left[\sum_{i=1}^N \delta(\mathbf{r} - \mathbf{r}_i) \exp \left[-\beta V(\mathbf{R}) + \beta \mu_M - \beta \sum_{i=1}^{N_m} \{ \psi_i(\mathbf{r}_i) + \lambda_i^{\text{el}}(\mathbf{r}_i) + \lambda_i^{\text{hchs}}(\mathbf{r}_i) \} \right] \right] \quad (16)$$

$$\rho_\alpha(\mathbf{r}) = \exp[\beta \mu_\alpha - \beta \{ \psi_\alpha(\mathbf{r}) + \lambda_\alpha^{\text{el}}(\mathbf{r}) + \lambda_\alpha^{\text{hchs}}(\mathbf{r}) \}] \quad (17)$$

where the effective fields, $\lambda_i^{\text{hchs}}(\mathbf{r})$ and $\lambda_i^{\text{el}}(\mathbf{r})$, from the hard

core and electrical contributions, respectively, on site i of the polyion, due to the presence of other polyions and small ions, are

$$\lambda_i^{\text{hchs}}(\mathbf{r}) = \frac{\delta F_{\text{hchs}}}{\delta \rho(\mathbf{r})} = f_{\text{hc}}(\bar{\rho}_{\text{hchs}}(\mathbf{r})) + \int d\mathbf{r}' \rho(\mathbf{r}') w(|\mathbf{r} - \mathbf{r}'|) f'_{\text{hc}}(\bar{\rho}_{\text{hchs}}(\mathbf{r}')) + \sum_\alpha \int d\mathbf{r}' \rho_\alpha(\mathbf{r}') w(|\mathbf{r} - \mathbf{r}'|) f'_{\text{hs}}(\bar{\rho}_{\text{hchs}}(\mathbf{r}')) \quad (18)$$

$$\lambda_i^{\text{el}}(\mathbf{r}) = \frac{\delta F_{\text{el}}}{\delta \rho(\mathbf{r})} = \int d\mathbf{r}' \frac{q_i \rho(\mathbf{r}')}{|\mathbf{r} - \mathbf{r}'|} + \sum_\alpha \int d\mathbf{r}' \frac{q_\alpha \rho_\alpha(\mathbf{r}')}{|\mathbf{r} - \mathbf{r}'|} \quad (19)$$

with $f'_{\text{hc}} = df_{\text{hc}}/d\rho$. Similarly, the effective fields on a small ion $\lambda_\alpha^{\text{hchs}}(\mathbf{r})$ and $\lambda_\alpha^{\text{el}}(\mathbf{r})$ are given by

$$\lambda_\alpha^{\text{hchs}}(\mathbf{r}) = \frac{\delta F_{\text{hchs}}}{\delta \rho_\alpha(\mathbf{r})} = f_{\text{hs}}(\bar{\rho}_{\text{hchs}}(\mathbf{r})) + \int d\mathbf{r}' \rho(\mathbf{r}') w(|\mathbf{r} - \mathbf{r}'|) f'_{\text{hc}}(\bar{\rho}_{\text{hchs}}(\mathbf{r}')) + \sum_\alpha \int d\mathbf{r}' \rho_\alpha(\mathbf{r}') w(|\mathbf{r} - \mathbf{r}'|) f'_{\text{hs}}(\bar{\rho}_{\text{hchs}}(\mathbf{r}')) \quad (20)$$

$$\lambda_\alpha^{\text{el}}(\mathbf{r}) = \frac{\delta F_{\text{el}}}{\delta \rho_\alpha(\mathbf{r})} = \int d\mathbf{r}' \frac{q_i \rho(\mathbf{r}')}{|\mathbf{r} - \mathbf{r}'|} + \sum_\alpha \int d\mathbf{r}' \frac{q_\alpha \rho_\alpha(\mathbf{r}')}{|\mathbf{r} - \mathbf{r}'|} \quad (21)$$

The electrical contributions originating from the direct Coulomb part⁴⁷ can be combined with the respective external potentials to give the respective mean electrostatic potentials, i.e.,

$$q_i \psi(\mathbf{r}) = \psi_i(\mathbf{r}) + \lambda_i^{\text{el}}(\mathbf{r}) \quad (22)$$

$$q_\alpha \psi(\mathbf{r}) = \psi_\alpha(\mathbf{r}) + \lambda_\alpha^{\text{el}}(\mathbf{r}) \quad (23)$$

where $\psi(\mathbf{r})$ is the mean electrostatic potential. Since the densities vary only along the z direction, Poisson's equation can be solved along with the appropriate boundary condition to obtain $\psi(z)$, which is given by

$$\psi(z) = -\frac{4\pi\sigma}{\epsilon} z - \frac{4\pi}{\epsilon} z \int_0^z dz' \left[\sum_{i=1}^{N_m} q_i \rho_{si}(z') + \sum_\alpha q_\alpha \rho_\alpha(z') \right] - \frac{4\pi}{\epsilon} \int_z^\infty dz' z' \left[\sum_{i=1}^{N_m} q_i \rho_{si}(z') + \sum_\alpha q_\alpha \rho_\alpha(z') \right] \quad (24)$$

Note that this satisfies the condition of overall electroneutrality, i.e.,

$$\int_0^\infty dz' \left[\sum_{i=1}^{N_m} q_i \rho_{si}(z') + \sum_\alpha q_\alpha \rho_\alpha(z') \right] + \sigma = 0 \quad (25)$$

The equations for the density profiles can now be written as

$$\rho(\mathbf{r}) = \int d\mathbf{R} \left[\sum_{i=1}^N \delta(\mathbf{r} - \mathbf{r}_i) \right] \exp \left[-\beta V(\mathbf{R}) + \beta \mu_M - \beta \sum_{i=1}^{N_m} \{q_i \psi(\mathbf{r}_i) + \lambda_i^{\text{hchs}}(\mathbf{r}_i)\} \right] \quad (26)$$

and

$$\rho_\alpha(\mathbf{r}) = \exp[\beta \mu_\alpha - \beta \{q_\alpha \psi(\mathbf{r}) + \lambda_\alpha^{\text{hchs}}(\mathbf{r})\}] \quad (27)$$

The DFT is completely specified through eqs 26 and 27 with the effective fields $\lambda_i^{\text{hchs}}(\mathbf{r})$ and $\lambda_\alpha^{\text{hchs}}(\mathbf{r})$ given by eqs 18 and 20, respectively, and the electrostatic potential given by eq 24. The presence of many-body function $V(\mathbf{R})$ on the right-hand side of eq 26 complicates the numerical implementation, which requires a single-chain simulation (or enumeration of conformations)³¹ at every step during the iterative solution.

In summary, the DFT starts with an expression for the free energy which is minimized with respect to the density profiles to give the density profiles and other static equilibrium properties. In the free energy functional, the ideal gas contribution is treated exactly, the hard sphere contribution is treated approximately but accurately, and the electrostatic contribution is treated using a van der Waals approximation. The theory goes beyond a mean field approximation in the sense that liquid-like correlations are taken into account, but the effect of electrostatic interactions on these correlations is neglected.

DFT predictions are obtained numerically as follows. We first generate an ensemble of chains in the presence of small ions. The chain conformations are generated so that each member of this ensemble appears according to the Boltzmann weight with only intramolecular interactions and interactions with small ions incorporated. An iterative method is then used to solve eqs 26 and 27 with the initial densities given by the modified Gouy–Chapman distribution.⁴⁸ The fields are obtained from eqs 18, 20, and 24, and a new estimate for the density profile is obtained from eqs 26 and 27. The single chain enumeration is carried out at each iteration with the same configurations generated initially with the assumption that the conformational properties of the polymer are not affected by other polyions or the surface. The numerical solution procedure must also satisfy the electro-neutrality condition at every iteration step. The iteration is continued until the convergence in the density profiles is achieved.

IV. Monte Carlo Simulation

Monte Carlo simulations are performed in the canonical ensemble (number of molecules, volume, and temperature constant). The system consisting of the polyions, counterions, and co-ions is confined in a rectangular parallelepiped ($Hd \times Ld \times Ld$) bounded on two sides by smooth flat surfaces in the z direction. We set $H = 2L$ in all cases, with H sufficiently large so that the solution in the middle region between the surfaces is uniform. Periodic boundary conditions are employed in the other two (x and y) directions. The degree of polymerization N_m is fixed as $N_m = 10$, and the number of chains, N_p , varies from 20 to 50 depending on the concentration. The simulations are performed for nominal polymer site densities, ρ_m^{av} , defined as $\rho_m^{\text{av}} d^3 = N_m N_p / L^2 H$ of 0.01, 0.06, 0.10, 0.15, and 0.2, and for surface charge densities of 0, 0.0625, 0.125, 0.25, and 0.5 e/d^2 in each case. The periodic length L varies from 8 for $\rho_m^{\text{av}} d^3 = 0.2$ to 28 for $\rho_m^{\text{av}} d^3 = 0.01$. The reduced bulk

density of polymer, required for theoretical calculations, is extracted by averaging the density profile in the middle of the cell where the fluid is uniform.

The simulation consists of three phases: initial configuration generation, equilibration, and averaging. The initial configuration is generated by random insertion of polyions, counterions, and coions into the simulation cell. In the equilibration phase, successive configurations are generated by a randomly chosen single particle move, chosen randomly between translation, reptation (slithering snake), and crank-shaft moves. In a straightforward application of the Metropolis algorithm,⁴⁹ a trial configuration is accepted with a probability, P_{acc} given as

$$P_{\text{acc}} = \min[1, \exp(-\beta \Delta U)] \quad (28)$$

where ΔU is the change in configurational potential energy of the system in going from the old to the new configuration. The two-dimensional Ewald sum is used to calculate the potential energy. The simulations are run for a total of 10^8 moves with approximately 10^6 moves for equilibration. Properties are averaged over 5–10 runs, each composed of 10^6 attempted moves, with the final configuration of one run used as the initial configuration for the next.

V. Results and Discussion

All polyion sites, counterions, and coions are monovalent and the system is at room temperature ($T = 298$ K) with water as the solvent, i.e., $\epsilon = 80$ and $l_B = 7.14$ Å. For convenience, the diameter of the hard spheres is chosen as the same as Bjerrum length and dimensionless quantities are used for the presentation, viz. z^* ($= z/d$) for distance, ρ^* ($= \rho d^3$) for density, σ^* ($= \sigma d^2/e$) for the surface charge density, ψ^* ($= \beta e \psi$) for the mean electrostatic potential. To compare to real experimental situations, each bead in our model corresponds roughly to two monomers in a vinyl polymer with the pair carrying a unit electronic charge, e .

In the simulations the nominal density of polymers, ρ_m^{av} , is kept fixed. This is because performing simulations at fixed bulk density requires grand canonical ensemble simulations, which are difficult for polymers. The theories, on the other hand, require the bulk polymer density, ρ_m , as input which we obtain from the simulations in the region where the density profile is uniform.

In solutions of neutral polymers, the polymer density profiles are governed by a competition between configurational and packing entropic effects which, respectively, result in a depletion and enhancement of polymer sites at the surface. Since spheres experience no loss of configurational entropy near the surface the value of the density of hard spheres at the surface is always greater than or equal to the bulk density. When the surfaces and species are charged, electrostatic effects compete with the above entropic effects. Since the polymers are attracted to the surface (as are the co-ions) and the counterions are repelled from the surface, the electrostatic effects tend to favor an accumulation of polymers and co-ions and a depletion of counterions at the surface.

Monte Carlo results for the density profiles of polyions, counterions, and co-ions are depicted in Figure 1a–c for $\rho_m^{\text{av}} d^3 = 0.1$, and $\sigma^* = 0.0625, 0.125$, and 0.25 , respectively. For the lowest charge density studied the polyion density profile shows a depletion in the immediate vicinity of the surface, a peak at $z^* \approx 2$, and then oscillatory behavior at larger separations. As the surface charge density is increased, the value of the density in the vicinity of the surface increases sharply, and the peak

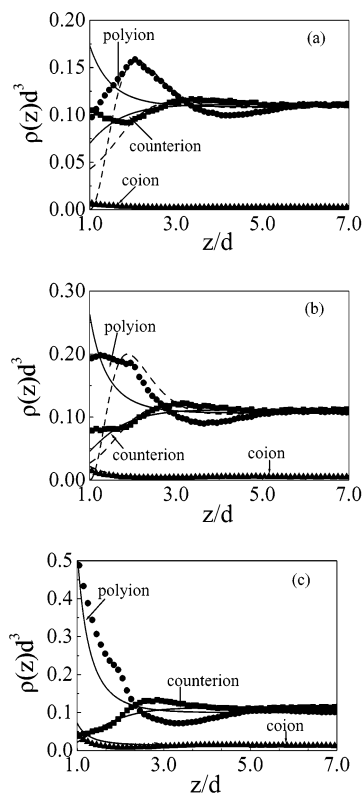


Figure 1. Monte Carlo simulation results (symbols), predictions of the density functional theory of this work (solid lines), and predictions of the theory of Shafir et al.¹⁹ (dashed lines) for the density profiles of the polyions, counterions, and co-ions for $\rho_m^{\text{av}}d^3 = 0.1$ and (a) $\sigma^* = 0.0625$, (b) $\sigma^* = 0.125$, and (c) $\sigma^* = 0.25$.

and valley move to slightly smaller distances, although this is not a very big effect. The oscillations in the density profiles are related to the liquid-like order (due to static correlations) present in dilute polyelectrolyte solutions and manifested in the peak in the static structure factor of these solutions at low concentrations.⁵⁰ Liquid-like ordering in solutions results in a liquid-like layering at a surface, and consequently oscillations in the density profile. The counterion density profile, on the other hand, displays a depletion at short distances followed by oscillatory behavior at larger distances. The depletion effect becomes more pronounced as the charge density is increased, but the magnitude and period of the oscillations do not change. The co-ion density is enhanced near the surface and there are oscillations in this density profile as well, although they are difficult to see because the co-ion density is very low at the charge densities studied. At high surface charge densities, the surface charge at the electrode is strongly screened by the polyion and consequently the oscillations are dampened toward the bulk value at a smaller distances. Note that at high surface charge densities the counterion density at the surface is lower than that of the co-ions, even though its bulk value is significantly higher. In all cases the counterion density is higher than the polymer density at intermediate separations. This phenomenon, often referred to as charge inversion, occurs on length scales of the order of $2-5d$ and moves to shorter distances as the surface charge density is increased.

Also shown (as solid lines) in Figure 1a–c are the predictions of the density functional theory. The theory predicts an accumulation of polyions and co-ions, and depletion of counterions at the surface, but the layering effects due to the correlation between the ions are absent. This is due to the fact that the present theory does not take into account the effect of

electrostatic interactions on the correlations between the ions which are clearly important³⁹ for these systems. However, the screening effects are quite reasonably captured by the present theory.

For comparison, we have also included (as dashed lines in Figure 1a and b), the predictions of the mean-field theory of Shafir et al.¹⁹ [We are unable to get converged results from this theory for higher surface charge densities.] Predictions from this theory are obtained by solving the two coupled nonlinear differential equations

$$\frac{d^2\psi^*(z)}{dz^2} = \kappa^2 \sinh \psi^*(z) - \kappa_m^2 (\exp(-\psi^*(z)) - \eta^2(z)) \quad (29)$$

$$\frac{1}{6} \frac{d^2\eta(z)}{dz^2} = \nu \phi_b^2 (\eta^3(z) - \eta(z)) - \psi^*(z) \phi(z) \quad (30)$$

where $\kappa = [(4\pi\beta/\epsilon)\sum_{\alpha} q_{\alpha}^2 \rho_{\alpha}^0]^{1/2}$, $\kappa_m = (4\pi l_B \phi_b^2)^{1/2}$, and $\eta(z) = \phi(z)/\phi_b$. In the above expressions, ρ_{α}^0 indicates the density of small ions at the bulk, $\phi_b^2 = c_b$ is the concentration of the polyion at the bulk, and $c(z) = \phi^2(z)$ represents the local concentration of the polyion. Following Shafir et al.¹⁹ the quantity ν is taken as 50 \AA^3 . The above equations are solved numerically using the relaxation method with the four boundary conditions. Two of them are the boundary values in the bulk, $z \rightarrow \infty$: $\eta(z) = 1$ and $\psi^*(z) = 0$, while the other two are the boundary values at the $z = 0$ surface and are given as $z \rightarrow 0$: $\eta(z) = 0$ and $d\psi/dz = -4\pi\sigma/\epsilon$. In the above, the concentration of the small ions are, however, determined by the usual Poisson–Boltzmann density distribution and are given by

$$\rho_{\alpha}(z) = \rho_{\alpha}^0 \exp(-\beta q_{\alpha} \psi(z)) \quad (31)$$

It can be seen in Figure 1a and 1b that even though the peaks in the density profile are quite well reproduced by the mean field theory, the density of the polyions is always zero at the surface. In addition, the predicted value of the counterion density at the surface is low when compared to the simulations and the DFT.

At a fixed surface charge density, the enhancement of polyion density at the surface increases as the polymer concentration is increased. Figure 2a–c depict the density profiles of polyions for $\rho_m^{\text{av}}d^3 = 0.01, 0.10, 0.15$, and 0.20 , and for $\sigma^* = 0.0625, 0.125$, and 0.25 , respectively. The MC simulation shows a significant accumulation of polyions at the surface as the concentration of the polyion increases, and this is also corroborated by the DFT. The layering effect becomes quite prominent at higher polyelectrolyte concentrations because of increased correlation at short distances. Increasing the surface charge density to $\sigma^* = 0.125$ leads to the adsorption of the polyions at the surface at a much lower concentrations (compare the curve for $\rho_m^{\text{av}}d^3 = 0.01$ in Figure 2b to the corresponding curve in Figure 2a) and this effect is even more pronounced for $\sigma^* = 0.25$. The DFT captures the increased adsorption reasonably well but fails to capture the correlation effects, which are important at these conditions. The mean field theory suffers from the drawback that the polyion density is zero at the contact, whereas it is quite high in the simulations (and the DFT).

The mean electrostatic potential profile provides us with a more direct comparison between the DFT and the theory of Shafir et al.¹⁹ Figure 3 depicts the mean electrostatic potential profiles for $\sigma^* = 0.0625$ and for $\rho_m^{\text{av}}d^3 = 0.01, 0.1, 0.15$, and 0.2 . The two theories predict different behavior: The mean electrostatic potential at the wall decreases in case of DFT,

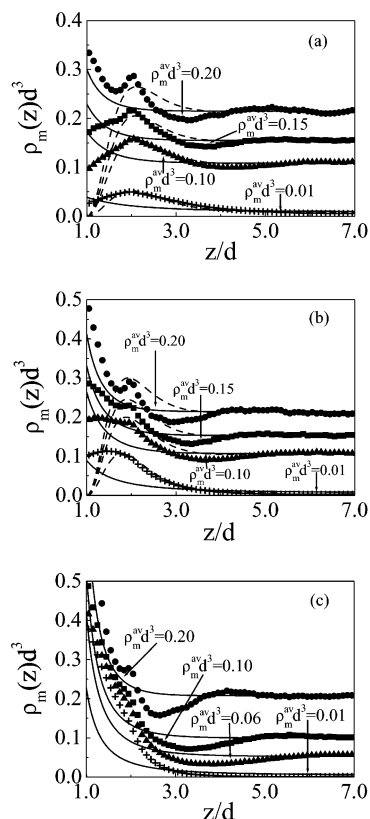


Figure 2. Comparison between DFT predictions (solid lines) and Monte Carlo simulations (symbols) for the density profiles of the polyions for various values of $\rho_m^{\text{av}} d^3$ (as marked) and surface charge densities of (a) $\sigma^* = 0.0625$, (b) $\sigma^* = 0.125$, and (c) $\sigma^* = 0.25$. Dashed lines are predictions of the theory of Shafir et al.¹⁹

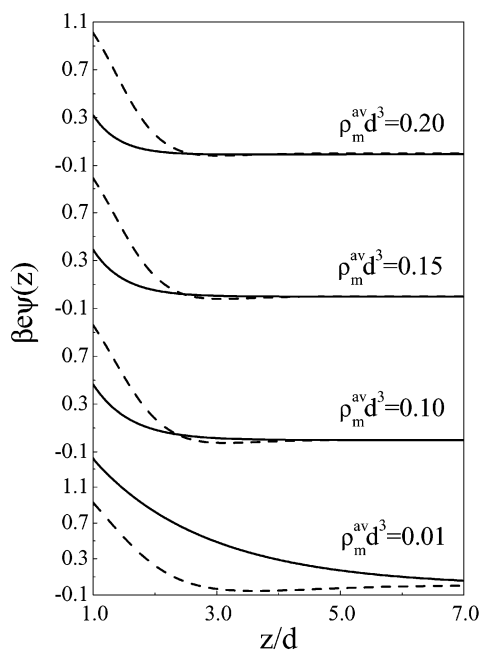


Figure 3. Density functional theory predictions (solid lines) and mean-field theory predictions (dashed lines)¹⁹ for the mean electrostatic potential profiles at $\sigma^* = 0.0625$ and for different polyion densities.

whereas it remains almost constant in case of mean-field theory. The dampening of correlation effects with increase in polyelectrolyte concentration, however, are quite well reproduced by both the DFT and the MFT. Similar behavior is also seen at a higher surface charge density of $\sigma^* = 0.125$ (not shown).

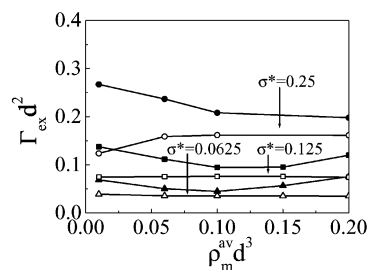


Figure 4. Comparison between DFT predictions (open symbols) and Monte Carlo simulations (filled symbols) for the surface excess Γ_{ex} as a function of $\rho_m^{\text{av}} d^3$ at various σ^* .

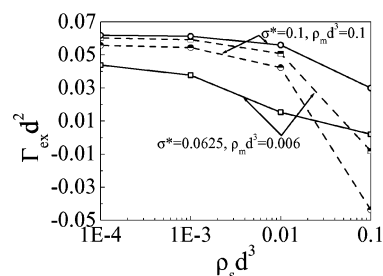


Figure 5. Comparison of DFT (open symbols) and MFT (mixed symbols)¹⁹ predictions for the variation of surface excess Γ_{ex} with added salt for two values of charge density and bulk polymer concentration (as marked). Lines are a guide to the eye.

A quantity of interest in experiments is the polymer surface excess, Γ_{ex} , defined as

$$\Gamma_{\text{ex}}^* = \Gamma_{\text{ex}} d^2 = \int_0^{H^*/2} [\rho_m^*(z^*) - \rho_m^*] dz^* \quad (32)$$

where ρ_m is the bulk polyion concentration. Figure 4 depicts Γ_{ex} as a function of polyion concentration for various surface charge densities. For highly charged surfaces, Γ_{ex} is quite high and more or less remains constant as the polyion concentration is increased. This behavior can be explained in terms of screening and excluded volume effects. As the polyion concentration is increased the screening between the ions and the surface is decreased. On the other hand, the volume exclusion causes the polyions to adsorb more strongly toward the surface. These opposite effects nullify each other at any polymer concentration, thereby keeping the surface excess more or less at a constant value. This shows that electrostatic interactions are not sufficient to explain the adsorption behavior even for this simple model, and excluded volume interactions begin to play an important role in semidilute solutions. As a consequence of the interplay between these two effects, Γ_{ex} displays a nonmonotonic variation with polymer density in most cases, both in the theory as well as in the simulations. While the trends predicted by the DFT as a function of charge density are in qualitative agreement with the simulations, the quantitative agreement is not as good. In all cases the DFT predicts an adsorption excess that is lower than what is seen in the simulations, and in some cases is in error by a factor of 2 or more.

The surface excess decreases with increasing added salt concentration in all cases. Figure 5 depicts DFT predictions for the variation of Γ_{ex} with added salt for two representative cases. In all cases, the surface excess decreases as the salt concentration is increased, because the electrostatic screening driving force for adsorption becomes weaker. This also suggests that the conditions of the system are within the “screening reduced” regime, as has been pointed out by van de Steeg et al.⁵¹

However, experiments point to the adsorption increase or decrease depending on the polyelectrolyte charge density^{52,53} and salt concentration,⁵⁴ which suggests that the experimentally observed behavior cannot be attributed solely to electrostatic effects.

VI. Concluding Remarks

The behavior of polyelectrolytes at surfaces is studied using density functional theory and Monte Carlo simulations. The polymer molecules are modeled as freely jointed chains of charged hard spheres, the counterions and co-ions as charged hard spheres, and the surface is taken as a planar, impenetrable hard wall containing uniform surface charge density. The density functional theory treats the hard chain contribution to the excess free energy functional using a weighted density approximation and the electrical contribution through the generalized van der Waals approximation. To our knowledge, this is the first such density functional study carried out for the polyelectrolyte solution in the presence of a surface.

The theory predicts density profiles of polyions, counterions, and co-ions that are in qualitative agreement with MC simulation results for a wide range of concentrations of the polyion and at various surface charge densities. For a fixed surface charge density, with increasing concentration of the polyion, the simulation predicts layering as well as charge inversion phenomena that are absent in the density functional theory. However, the increase in the surface concentration of polyions with increasing bulk concentration is quite well reproduced by the theory. The surface excess of the polyion increases with increasing surface charge density, although it remains more or less constant with the polyion concentration because of competing effects from electrostatic screening and excluded volume.

It is highly encouraging to note that the theory provides results comparable with Monte Carlo simulation even though only a simple van der Waals approximation is used for the direct Coulomb contribution. However, the theory is unable to capture the correlation effects. This is mainly because we have neglected the correlation between the hard sphere and the Coulomb interactions. In fact, a more rigorous theory can be proposed for the present system to include the coupling term along with the present prescription, as was done recently³⁷ for attractive chains at surfaces. It is of interest to investigate the effect of polymer architecture, counterion and co-ion valence, and solvent effects on the adsorption behavior. These phenomena are possible to study within the framework of DFT studied here, although it will be important to account for the coupling of hard sphere and electrostatic correlations in a more rigorous fashion. Work along these directions is in progress in our laboratory.

Acknowledgment. This material is based upon work supported by the National Science Foundation under Grant No. CHE-0315219. C. N. P. thanks Dr. Swapan K. Ghosh and Dr. T. Mukherjee for their kind interest and constant encouragement.

References and Notes

- (1) *Polyelectrolytes: Science and Technology*; Hara, M., Ed.; Dekker: New York, 1993.
- (2) Decher, G. *Science* **1997**, 277, 1232.
- (3) Hartgerink, J. D.; Beniash, E.; Stupp, S. I. *Science* **2001**, 294, 1684.
- (4) Rädler, J.; Koltover, I.; Salditt, T.; Safiyna, C. *Science* **1997**, 275, 810.
- (5) Fang, Y.; Yang, J. *J. Phys. Chem. B* **1997**, 101, 441.
- (6) Jary, D.; Sikorav, J.-L. *Biochemistry* **1999**, 38, 3223.
- (7) Shimomura, M.; Sawadaishi, T. *Curr. Opin. Coll. Interface Sci.* **2001**, 6, 11.
- (8) Gittins, D. I.; Caruso, F. *J. Phys. Chem. B* **2001**, 105, 6846.
- (9) Dahane, L.; Leporatti, S.; Donath, E.; Mohwald, H. *J. Am. Chem. Soc.* **2001**, 123, 5431.
- (10) Sullivan, D. M.; Bruening, M. L. *J. Am. Chem. Soc.* **2001**, 123, 11805.
- (11) Thierry, B.; Winnik, F. M.; Merhi, Y.; Tabrizian, M. *J. Am. Chem. Soc.* **2003**, 125, 7494.
- (12) Monteux, C.; Williams, C. E.; Meunier, J.; Anthony, O.; Bergeron, V. *Langmuir* **2004**, 20, 57.
- (13) Muthukumar, M. *J. Chem. Phys.* **1987**, 86, 7230.
- (14) Joanny, J.-F. *Eur. Phys. J. B* **2000**, 9, 117.
- (15) Borukhov, I.; Andelman, D.; Orland, H. *J. Phys. Chem. B* **1999**, 103, 5042.
- (16) Borisov, O. V.; Zhulina, E. B.; Birshtein, T. M. *J. Phys. II France* **1994**, 4, 913.
- (17) Dobrynin, A. V.; Deshkovsky, A.; Rubinstein, M. *Phys. Rev. Lett.* **2000**, 84, 3101.
- (18) Netz, R. R.; Andelman, D. *Phys. Rep.* **2003**, 380, 1.
- (19) Shafir, A.; Andelman, D.; Netz, R. R. *J. Chem. Phys.* **2003**, 119, 2355.
- (20) van der Schee, H. A.; Lyklema, J. *J. Phys. Chem.* **1984**, 88, 6661.
- (21) Böhmer, M. R.; Evers, O. A.; Scheutjens, J. M. H. M. *Macromolecules* **1990**, 23, 2288.
- (22) Shew, C.-Y.; Yethiraj, A. *Phys. Rev. Lett.* **1996**, 77, 3937.
- (23) *Computer Simulations of Polymers*; Roe, R. J., Ed.; Prentice Hall: Englewood Cliffs, NJ, 1991.
- (24) Fleer, G. J.; Cohen-Stuart, M. A.; Schetjens, J. M. H.; Cosgrove, T.; Vincent, B. *Polymers at Interfaces*; Chapman and Hall: London, 1993.
- (25) Yoon, D. Y.; Vacatello, M.; Smith, G. D. In *Monte Carlo and Molecular Dynamics Simulations in Polymer Science*; Binder, K., Ed.; Oxford University Press: New York, 1995.
- (26) Yethiraj, A. *Phys. Rev. Lett.* **1997**, 78, 3789.
- (27) Shew, C.-Y.; Yethiraj, A. *J. Chem. Phys.* **1999**, 110, 11599.
- (28) Micka, U.; Kremer, K. *Europhys. Lett.* **2000**, 49, 189.
- (29) Liu, S.; Muthukumar, M. *J. Chem. Phys.* **2002**, 116, 9975.
- (30) Liu, S.; Ghosh, K.; Muthukumar, M. *J. Chem. Phys.* **2003**, 119, 1813.
- (31) Yethiraj, A.; Woodward, C. E. *J. Chem. Phys.* **1995**, 102, 5499.
- (32) Szleifer, I.; Carignano, M. A. *Adv. Chem. Phys.* **1996**, 94, 742.
- (33) Yethiraj, A. *J. Chem. Phys.* **1998**, 109, 3269.
- (34) Hooper, J. B.; McCoy, J. D.; Curro, J. G. *J. Chem. Phys.* **2000**, 112, 3090.
- (35) Yethiraj, A. *Adv. Chem. Phys.* **2002**, 121, 89.
- (36) Patra, C. N.; Yethiraj, A. *J. Chem. Phys.* **2000**, 112, 1579.
- (37) Patra, C. N.; Yethiraj, A. *J. Chem. Phys.* **2003**, 118, 4702.
- (38) Yu, Y.-X.; Wu, J. *J. Chem. Phys.* **2002**, 117, 2368.
- (39) Patra, C. N.; Yethiraj, A. *J. Phys. Chem. B* **1999**, 103, 6080.
- (40) Patra, C. N.; Yethiraj, A. *Biophys. J.* **2000**, 78, 699.
- (41) McMullen, W. E.; Freed, K. F. *J. Chem. Phys.* **1990**, 92, 1413.
- (42) Woodward, C. E. *J. Chem. Phys.* **1991**, 94, 3183.
- (43) Stell, G. In *The Equilibrium Theory of Classical Fluids*; Frisch, H. L., Lebowitz, J. L., Eds.; W. A. Benjamin: New York, 1964.
- (44) Nordholm, S.; Johnson, M.; Freasier, B. C. *Aust. J. Chem.* **1980**, 33, 2139.
- (45) Hansen, J. P.; McDonald, I. R. *Theory of Simple Liquids*; Academic: New York, 1986.
- (46) Woodward, C. E.; Yethiraj, A. *J. Chem. Phys.* **1994**, 100, 3181.
- (47) Patra, C. N.; Ghosh, S. K. *J. Chem. Phys.* **2002**, 117, 8938.
- (48) Carnie, S. L.; Torrie, G. M. *Adv. Chem. Phys.* **1984**, 56, 141.
- (49) Metropolis, N.; Rosenbluth, A. W.; Rosenbluth, M. N.; Teller, A. H.; Teller, E. *J. Chem. Phys.* **1953**, 21, 1087.
- (50) Yethiraj, A. *J. Chem. Phys.* **1999**, 111, 1797.
- (51) van de Steeg, H. G. M.; Cohen Stuart, M. A.; de Keizer, A.; Bijsterbosch, B. H. *Langmuir* **1992**, 8, 2538.
- (52) Davies, R. J.; Dix, L. R.; Toprakcioglu, C. *J. Colloid Interface Sci.* **1989**, 129, 145.
- (53) Orlando, J. R.; Ernstsson, M.; Neuman, R. D.; Claesson, P. M. *Langmuir* **2002**, 18, 1604.
- (54) Shubin, V.; Linse, P. *J. Phys. Chem.* **1995**, 99, 1285.